SPATIALLY-DISTRIBUTED SNOWMELT RATES IN A BOREAL FOREST BASIN

Metcalfe[1], R.A., and Buttle[2], J.M.

ABSTRACT

Spatial variation in snowmelt rates in the boreal forest can be explained by differences in canopy density. Canopy density, represented as gap fractions (GF), controls both the amount of shortwave radiation reaching the snowpack surface and wind speed over the snow surface, which in turn regulates sensible and latent heat fluxes. These reductions outweigh any increased contributions from longwave radiation as a result of increased biomass. Differences in the total energy available for melt do not translate to equally proportional changes in melt rates under different canopy densities. As available energy increases, the melt rate increases with decreasing canopy density and the form of the relationship can vary depending on climatic conditions. A good relationship between ground-based GF measurements and a canopy closure index derived from Landsat TM, provides the spatial fabric for the physically-based distribution of snowmelt rates that shows comparable patterns of snow ablation during years of very different climatological conditions. This physically-meaningful method of determining the spatial variability of meltwater delivery to the soil interface provides a better understanding of the heterogeneous active layer development and runoff processes in the boreal forest.

INTRODUCTION

Snowmelt is the most significant hydrologic event in the boreal forest biome. Not only is it an important component of the annual water balance, but its duration and timing exert strong controls over net primary production of the boreal forest and exchanges of energy and carbon. The focus of the Boreal Ecosystem-Atmosphere Study (BOREAS) is to elucidate interactions between energy and mass between the boreal forest biome and the lower atmosphere to clarify their roles in global change (Sellers *et al*, 1995). Of particular importance to BOREAS is a better understanding of physical processes governing these exchanges. This will lead to improved process models that can be used to test remote sensing algorithms in an attempt to scale up point measurements in order to apply them to larger spatial scales. This study focuses on spatial variation in snowmelt rates in a boreal forest basin under the premise that the heterogeneity of meltwater delivery to the soil interface results in spatially-variable development of the active layer, and that this variability must be elucidated to enable a full understanding of the runoff processes in the boreal forest.

Spatial variation in snow accumulation and ablation has been linked to such parameters as slope angle and aspect (e.g. Hendrick *et al.*, 1971; Price and Dunne, 1976; Buttle and McDonnell, 1987), terrain units (e.g. Woo and Marsh, 1978), vegetation cover (e.g. FitzGibbon and Dunne, 1983), and land use (e.g. Adams, 1976; Burkhard *et al.*, 1991). The low relief of the boreal forest results in vegetation properties being the primary control over snow accumulation and energy exchanges responsible for snowmelt (Metcalfe and Buttle, 1995; Hardy *et al.*, 1997; Davis *et al.*, 1997). In this study, canopy density is assumed to be the vegetative property exerting the greatest control over snowmelt rates. Canopy density characteristics are obtained through ground-based gap fraction (GF) measurements, the fraction of sky visible to a sensor placed beneath a canopy. When related to a canopy closure index (CCI) derived from Landsat Thematic Mapper (TM) imagery, GF values can be used to provide the spatial fabric to distribute snowmelt rates in the boreal forest. The physical basis for this hypothesis is that canopy density controls both the solar radiation flux (K↓) reaching the snowpack and wind speed over the snowpack surface, which in turn controls sensible and latent heat fluxes (Q_H and Q_E). The reduction in these energy components is assumed to outweigh any increases in longwave radiation (L↓) directed toward the snowpack because of increased biomass associated with greater canopy density; an assumption supported by Davis *et al.* (1997). Therefore, increased canopy density (decreased GF) is associated with decreased snowmelt rates.

STUDY AREA AND METHODS

The study was conducted in a small (2.4 km^2), low-relief drainage basin in the boreal forest 40 km northwest of Thompson, Manitoba (55° 55.5'N, 98° 25'W, Figure 1). The basin discharges to a larger fen (a BOREAS tower flux measurement site), and consists of low-angle slopes draining to a system of interconnected wetlands. The gently rolling terrain, extending from 253 m to 276 m a.s.l., is underlain by discontinuous permafrost and covered primarily by black spruce (*Picea mariana*), with lesser amounts of white birch (*Betula papyrifera*), larch (*Larix laricina*), *Populus* spp., and jack pine (*Pinus banksiana*) on the better-drained soils. Ground cover on the better drained soils of the open forested areas is dominated by *Cladina* spp., particularly reindeer lichen (*C. rangiferna*), with an overstory of labrador tea (*Ledum groenlandicum*). In areas with more closed forest cover and higher soil moisture, these species are mixed with feather moss (*Pleurozium schreberi*), sphagnum mosses (*Sphagnum* spp.), and some scrub birch (*Betula glandulosa*) and willow (*Salix* spp.), with the latter more prominent at wetland fringes. Characteristic wetland species include sedges (*Carex* spp.), mosses (*Sphagnum* spp.) and bog laurel (*Kalmia* spp.). The fen to the south of the basin has a sparse overstory of bog birch (*Betula glandifera*), larch and black spruce, and an understory of buckbean (*Menyanthes trifoliata*), sedges and cotton grass (*Eriophorum augustifolium*). Wetlands contain typic and humic mesisols, while the hillslopes are mantled by orthic grey luvisols and orthic lutric brunisols. Mean annual precipitation for the basin is ~ 0.45 m, mean annual snowfall is ~ 1.7 m, mean January daily temperature is ~ -25°C and mean July daily temperature is ~ 16°C (Hydrological Atlas of Canada, 1978).

[1]*Department of Geography, Queen's University, Kingston, Ontario, Canada, K7L 3N6*

[2]*Department of Geography, Trent University, Peterborough, Ontario, Canada, K7L 7B8*

The spatial distribution of snow water equivalent (SWE) was determined prior to spring melt by a 62-point snow survey in 1994 and a 64-point snow survey in 1995. A stratified sample was acquired by classifying the catchment with respect to dominant vegetation types. These units included open wetland, wetland with willow, open black spruce, open mixed forest, close mixed forest, and closed black spruce, with 'open' and 'closed' being a qualitative measure of relative canopy density of the site. Since variability in snow depth generally exceeds that of snow density, each sampling site consisted of one snow density and one depth measurement taken at a central location supplemented by four snow depth measurements taken 2 m away in each of the cardinal directions. Snow densities were determined using an Atmospheric Environment Service (AES) snow tube to obtain a snow sample that was placed in a polyethylene bag and later weighed. Mean snow depth, density, and SWE were recorded at each site.

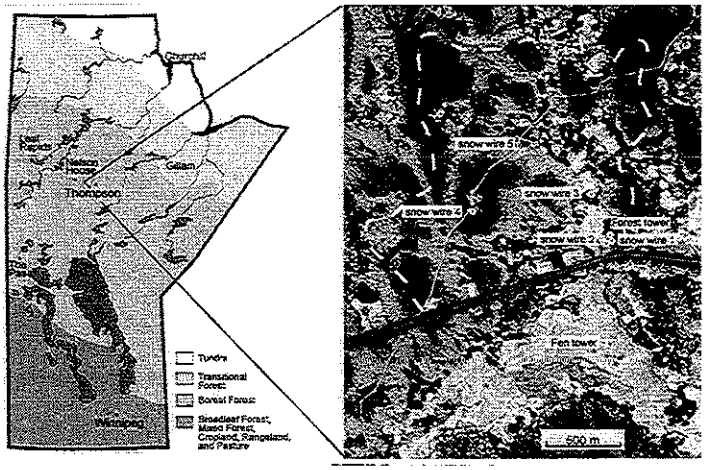

Figure 1 Study basin location and instrumentation (air photo taken on DOY 110, 1994).

The LAI-2000 plant canopy analyzer (LI-COR Inc., Lincoln, Nebraska - Welles and Norman, 1991), provided an indirect measure of canopy structural characteristics at each snow-wire. Measurements are presented as gap fractions ranging between 0 (no sky visible to the sensor) and 1 (no foliage visible to the sensor). Gap fractions were determined by using one LAI-2000 unit to record above-canopy sky brightness at 30 s intervals while another unit was used to record below-canopy readings at the snow-wires. Below-canopy readings were then compared to the nearest above canopy readings in time. Above-canopy readings for snow-wires 1 to 5 were taken on top of a van parked in a clearing at the basin outflow. Above-canopy readings for the fen snow-wire were taken on the roof of a building at the site. Measurements were taken after sunset, before sunrise, or during overcast periods when the sky brightness was closest to optimal (i.e. uniform), to minimize the potential error caused by the distance between the two sensors. Errors caused by direct sunlight on the sensor or sunlit portions of the canopy (both resulting in an overestimation of the GF) were also minimized at these times. Canopy heterogeneity warranted use of 90° view caps on the sensors; therefore, one measurement was taken in each of the four cardinal directions and averaged to obtain the gap fraction for each snow-wire. Sensors were calibrated prior to measurement, and were aligned in the same cardinal direction during measurement to ensure that both sensors were viewing the same portion of the sky. All measurements were taken at a mean height of 0.4 m above the ground surface. Gap fraction values for each of the snow-wires are given in Table 1.

Daily snowmelt was measured using the snow-wire technique (Heron and Woo 1978, Figure 2). A taut horizontal wire 1.75 - 2.0 m in length was suspended over the snowpack surface. The distance from the wire to the snowpack surface (z) was measured at 0.1 m intervals over a distance of 1 m along the central portion of the wire prior to the daily melt cycle. Three samples of the surface snow density (ρ_s) were obtained concurrently using 250 cm^3 snow cores extracted parallel to the surface. Melt was determined from:

$$M = \overline{\Delta z} \times \overline{\rho_s} \qquad (1)$$

where M = daily melt (mm)
$\overline{\Delta z}$ = mean change in the distance from the wire to the snowpack surface between times t and $t+\Delta t$ (m)
$\overline{\rho_s}$ = mean density of surface snow layer at time t (kg m^{-3})

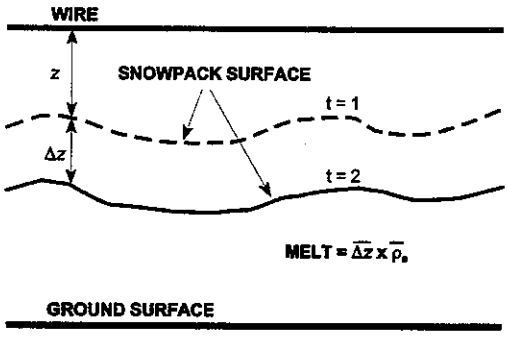

Figure 2 The snow-wire method of estimating melt.

The standard error associated with the mean melt depth was determined as:

$$s.e._M = \sqrt{s.e._{\Delta z}^{\,2} \times \overline{\rho_s}^{\,2} + s.e._{\rho_s}^{\,2} \times \overline{\Delta z}^{\,2}} \qquad (2)$$

where $s.e._M$ = standard error of the mean melt depth (mm)
$s.e._{\rho s}$ = standard error of the mean snowpack density (kg m^{-3})
$s.e._{\Delta z}$ = standard error of Δz (m)

Five snow-wires were deployed in the dominant vegetation units in the basin prior to melt, while a sixth was installed in the fen south of the basin (Figure 1). Snow-wires 1, 3, 4, 5 were in the same locations for both years while the fen snow-wire and snow-wire 2 were moved a few meters in 1995 to take advantage of areas of greater snow accumulation in an effort to prolong the measurement series.

To acquire information about the climatological conditions during springmelt and to enable calculation of the energy components responsible for snowmelt, instrumentation was installed on two micrometeorological towers: one in the centre of the fen south of the basin to represent an 'open' area (fen snow-wire), and one in a forest stand within the basin (snow-wire 1)(see Figure 1). Energy fluxes responsible for snowmelt were obtained from solution of the snowpack's energy balance:

$$Q_M = Q^* + Q_H + Q_E + Q_G + Q_P - Q_\theta \quad (3)$$

where Q_M = energy available for melt (W m^{-2})
Q^* = net radiation (W m^{-2})
Q_H = sensible heat flux (W m^{-2})
Q_E = latent heat flux (W m^{-2})
Q_G = ground heat flux (W m^{-2})
Q_P = energy flux delivered to the snowpack by rainfall (W m^{-2})
Q_θ = change in negative heat storage in the snowpack (W m^{-2})

Q^* was measured directly using Middleton net radiometers while the bulk transfer approach (Heron and Woo, 1978; Price, 1988) was used to calculate convective and latent energy exchanges (Q_H and Q_E) using measurements of wind speed, temperature and relative humidity. Instrumentation at both towers was positioned 2 m above the initial snowpack surface except at the fen tower where the net radiometer and instrumentation to measure the full radiation balance were positioned 10 m above the ground surface. Downward soil temperature gradients were observed at both sites during melt, such that Q_G was ignored. Tipping bucket rain gauges recorded rainfall near each tower and Q_P contributions were estimated assuming that rainfall temperature equalled concurrent air temperature. Q_θ was approximated by summing nocturnal Q^* losses from the snowpack, and initial positive Q^* fluxes the following day were used to satisfy this cumulative heat deficit. When Q_θ equalled 0, the snowpack was assumed to be isothermal at 0°C and any further energy inputs contributed directly to Q_M. Either Q_M, which is always positive, or Q_θ, which is always negative, must be 0 at all times. All measurements were recorded on Campbell data loggers and Q_M was estimated based on hourly averages. Snow-depth was also recorded at the forest tower every 15 minutes using an ultrasonic snow depth sensor.

Thermocouples were placed in the snowpack at both tower sites to detect when the snowpack became isothermal. In 1994, snowpack temperatures were recorded using thermocouples inserted into holes drilled at 0.1 m intervals along a wooden dowel painted white and erected the previous autumn. Wire was wound around the dowel at each thermocouple location to minimize the effect of heat conduction down the wire and then placed in grooves along the dowel and siliconed to prevent water seepage. In 1995, snowpack temperatures were recorded using thermocouples that extended from wooden dowels and inserted horizontally into the settled snowpack at 0.10 m intervals.

Delineation of the basin divide, identification of sampling locations, and georeferencing of the TM imagery was achieved using a digital video plotter and 1:15,840 digital stereo photographs scanned at 1000 dots per inch (dpi).

RESULTS AND DISCUSSION

Pre-melt SWE

Mean snow depth, density and SWE for each vegetation type are presented in Table 1. SWE values for both years for the open mixed forest and open black spruce units as well as the mixed forest and black spruce units were not significantly different at $\alpha = 0.05$ using Tukey's multiple means comparison, and therefore have been aggregated. Also, SWE values for the wetland with willow and open forested units were not significantly different; however, they are presented separately for purposes of deriving a spatially-distributed SWE for the basin discussed below.

The higher snow densities, and to some extent lower snow depths, measured in 1995 resulted from pre-melt snowpack metamorphism and settling during a period of warm air temperatures from Day of Year (DOY) 79 to DOY 86 (discussed below). Comparable warm periods were absent in 1994 and snowpack metamorphism was largely restricted to the initiation of springmelt. The least SWE in both years was recorded in forested areas, where interception and sublimation resulted in SWE losses, and in open wetlands, where wind redistributed snow to the wetland fringes. The greatest SWE was recorded in the wetland with willow and open forest units. This is the result of the more open canopies causing airflow perturbations over the canopy, thus enhancing snow deposition as well as limiting snowfall interception and subsequent sublimation (Schmidt, 1991). The wetland with willow would also accumulate redistributed snow from open wetland areas. Differences in mean SWE between vegetation units were consistent for both years as were the differences in mean SWE of the same vegetation unit between years. Mean SWE over all the vegetation units decreased by 0.022 m from 1994 to 1995.

Climatic conditions during melt

Meteorological observations from the two towers for the 1994 and 1995 melt seasons are shown in Figures 3a, 3b, 4a, and 4b, respectively. Notable differences are the higher air temperatures and windspeeds in 1994 as well as the greater fluctuations in air temperature. The effect of forest canopy on windspeed is clearly evident as is the effect of the canopy on incoming shortwave radiation shown by the 'spikes' in Q^*.

Table 1 Canopy and pre-melt mean snowpack characteristics (± 1 s.d.) for dominant vegetation types.

Vegetation Type		open wetland	wetland with willow	open mixed forest and open black spruce	mixed forest and black spruce
% of basin		4	7	41	48
Snow-wires		2	Fen	3, 5	1, 4
Gap fractions at snow-wires		0.992	0.971	0.459, 0.659	0.268, 0.063
Depth (m)	1994	0.571 ± 0.087 n = 30	0.674 ± 0.049 n = 45	0.660 ± 0.094 n = 125	0.526 ± 0.094 n = 110
	1995	0.329 ± 0.108 n = 35	0.488 ± 0.078 n = 45	0.454 ± 0.065 n = 125	0.305 ± 0.090 n = 110
Density ($kg\ m^{-3}$)	1994	202 ± 38 n = 6	203 ± 17 n = 9	202 ± 22 n = 25	192 ± 36 n = 22
	1995	282 ± 27 n = 7	238 ± 45 n = 9	249 ± 36 n = 25	257 ± 44 n = 22
SWE (m)	1994	0.113 ± 0.009	0.136 ± 0.007	0.133 ± 0.022	0.100 ± 0.020
	1995	0.091 ± 0.023	0.114 ± 0.019	0.112 ± 0.018	0.078 ± 0.027

Snow-wire measurements and meteorological observations at both towers began on DOY 100 in 1994. Maximum daily air temperatures were above 0°C immediately preceding this date; however, low nocturnal air temperatures delayed warming of the snowpack. The snowpack became isothermal by the afternoon of DOY 101, resulting in rapid initiation of melt. Melt then became more gradual with greater nocturnal cooling of the pack and ceased completely between DOY 113 and DOY 116 when air temperatures remained below 0°C. Increasing air temperatures beginning DOY 117 quickly warmed the pack and reinitiated melt.

Air temperatures recorded in 1995 at the Saskatchewan Research Council's meteorological tower at the Old Jack Pine tower flux site (15 km west of the basin) indicated maximum daily air temperatures of 4°C to 9°C from DOY 78 to DOY 86 with associated nocturnal temperatures barely reaching -4°C. Some snow cover may have melted during this time, and the pack certainly underwent metamorphism resulting in the higher snowpack densities observed in the snow survey relative to 1994 (Table 1). Snow-wire measurements and observations at the forest tower began on DOY 99 while the fen tower became fully operational on DOY 100. Melt began on DOY 99 but ceased during a cool period between DOY 106 and DOY 110. The pack warmed again between DOY 111 and DOY 114 as daily maximum air temperatures consistently reached 4°C and nocturnal cooling decreased. Melt stopped again on DOY 115 and DOY 116 due to a decrease in $K\downarrow$ combined with lower daily air temperatures. Meltrates then increased beginning DOY 117 due to greater daily maximum air temperatures and reduced nocturnal cooling.

Comments on the snow-wire method

The depth of a ripening snowpack can decrease considerably through gravitational settling and melt metamorphism. Snow-wire measurements taken during this stage would overestimate melt (Heron and Woo, 1978), since the decrease in depth (Δz) is not associated with meltwater actually leaving the snowpack. Changes in snow density and snow depth can act as surrogate indicators of melt initiation, which is best detected by snowpack temperature measurements. Surface snow density measurements recorded at the snow-wires for both years show densities increased during warming and ripening and remained relatively constant throughout the ablation period (Figure 5). Departures were the result of deposition of less dense snow on the pack surface during snowfall (e.g. DOY 116-117, 1995), and several days elapsed before surface densities retained those of ripe snow. Thermocouple measurements in 1994 indicated the snowpack became isothermal late DOY 101. Surface snowpack densities rose through DOY 103 (Figure 5) and snow depth decreased ca. 0.1 m (Figure 6) as temperatures remained high. Snowmelt calculations began on DOY 102. In 1995 the snowpack became isothermal and melt was initiated on DOY 101, consistent with increased snow surface density (Figure 5) and decreased snowpack depth (Figure 6).

Density of the upper layer of the snowpack can vary vertically over short distances due to the presence of ice lenses and fresh snowfall, and the effect of such variations on the snow density measurements used in the melt calculations was examined. Ideally, density measurements should integrate over the depth of snow that would be ablated that day. However, this was seldom observed, given the fixed width of the snow sampler used to measure density. Snow densities obtained using the 250 cm^3 snow sampler (6.0 cm diameter) were compared with values obtained using a 100 cm^3 snow sampler (4.7 cm diameter) on DOY 118-123 in 1994 at snow-wires 1, 3, 4, and 5. Three samples were

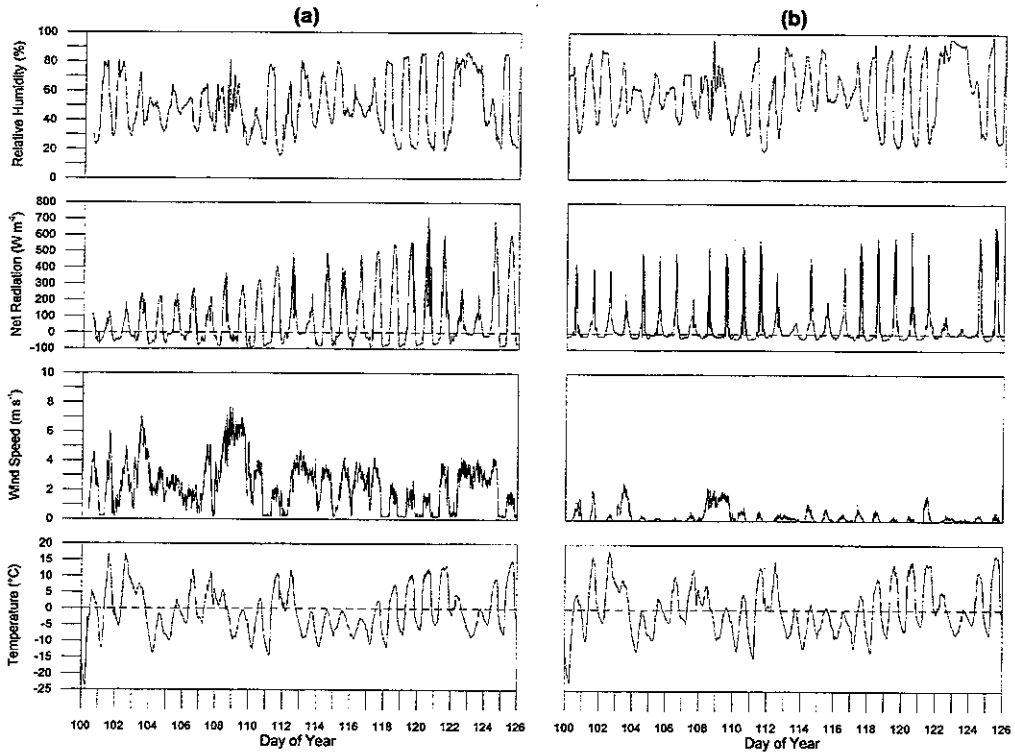

Figure 3 Micrometeorological observations at the (a) fen and (b) forest towers during the 1994 snowmelt period.

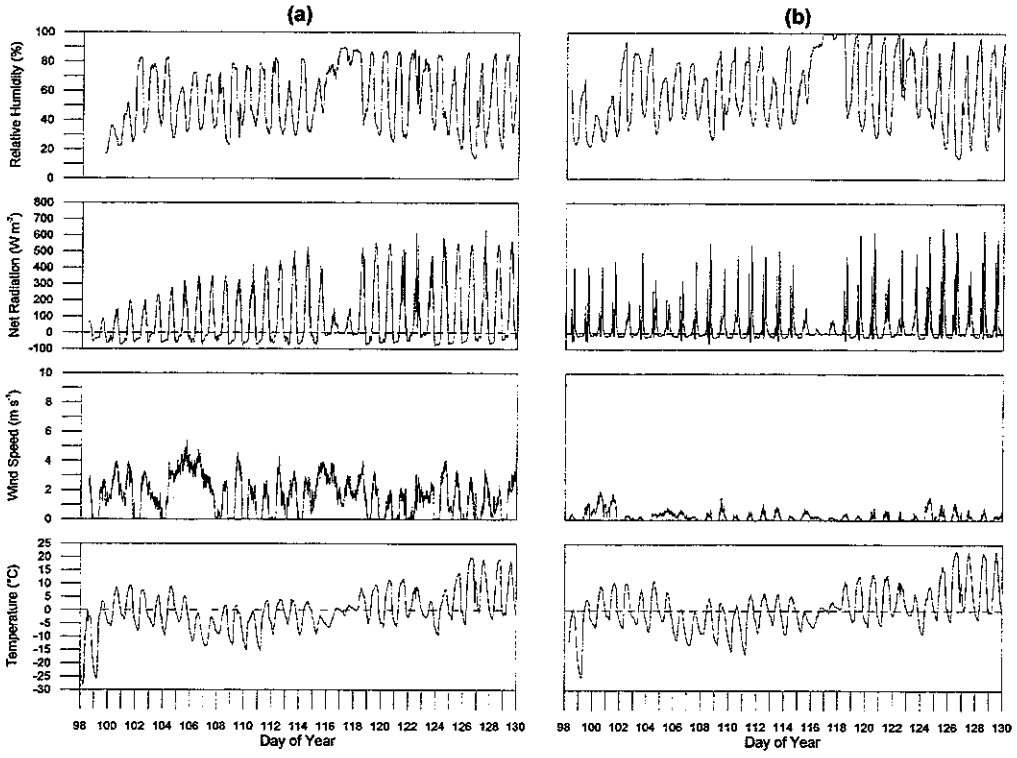

Figure 4 Micrometeorological observations at the (a) fen and (b) forest towers during the 1995 snowmelt period.

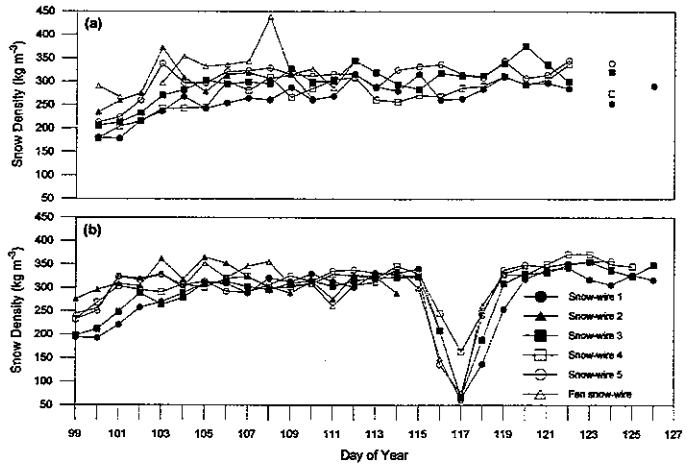

Figure 5 Surface snow density measurements measured at the snow-wires for (a) 1994 and (b) 1995.

obtained at each wire using each snow sampler, and a paired t-test found no significant difference between the mean snow densities at $\alpha = 0.05$. Differences were most pronounced after deposition of a layer of fresh snow thicker than the diameter of the 100 cm^3 sampler but smaller than that of the 250 cm^3 sampler. As a result, the latter incorporated older, denser snow in the density estimate.

Snowmelt estimates from the snow-wire method

Loss of continuous snow cover below some snow-wires at the end of the 1994 and 1995 melt periods limited calculation of snowmelt rates to the days shown in Figure 7, which indicates substantial and consistent variability in melt between sites. Snow in the open sites (fen and snow-wire 2) ablated much faster than in the forest. However, melt differed between sites that might otherwise have been considered similar (Figure 8). Although the fen and snow-wire 2 have almost identical GF values and might be considered to represent "open" areas

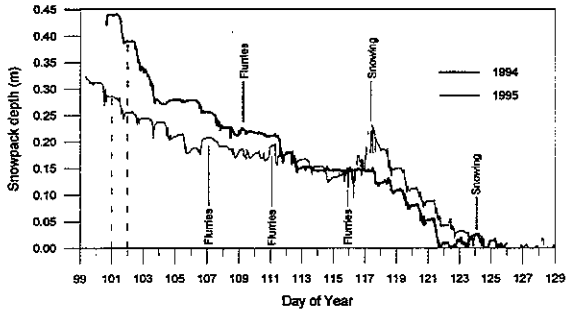

Figure 6 Snow depth measurements recorded at the forest tower for both field seasons. Periods of pronounced depth oscillations were caused by falling snow.

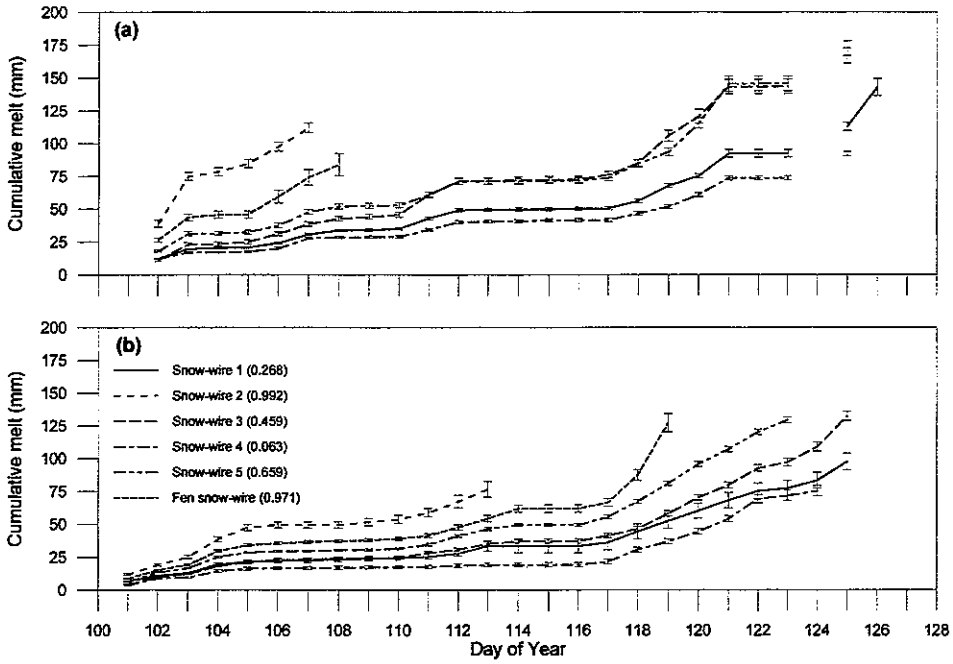

Figure 7 Cumulative snowmelt measured at the snow-wires in (a) 1994 and (b) 1995, ± 1 standard error about the mean melt depth.

in a lumped model, the sparse canopy within the fen and along wetland margins apparently affected snow ablation as well as snow accumulation (Table 1). Melt differences were most prominent for DOY 102 and 103 in 1994, and may have resulted from dust contributions from Highway 391 to the snow-wire 2 snowpack, thus lowering the albedo and enhancing melt. Other possible explanations for the higher meltrates at snow-wire 2 may include: (1) the effect of the fen overstory, which would reduce wind speeds and turbulent fluxes relative to the more open site at snow-wire 2; (2) greater advection of sensible heat from the surrounding forest at snow-wire 2 relative to the fen site, which was less susceptible to boundary influences owing to its greater fetch; and (3) greater penetration of solar radiation to the vegetation underlying the shallower snowpack at snow-wire 2 (Koh and Jordan, 1995).

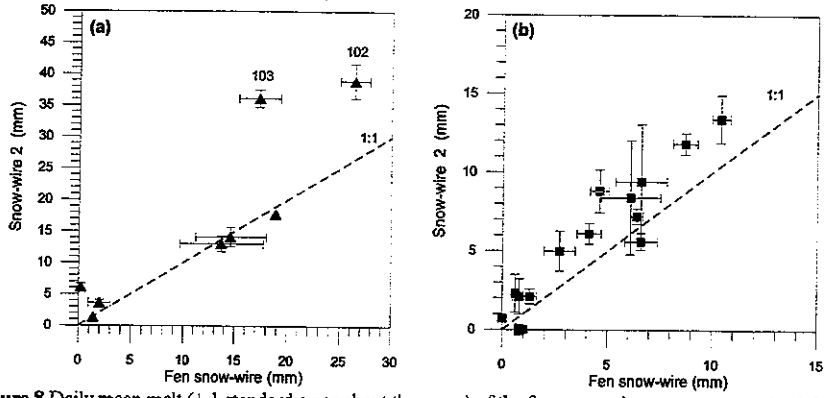

Figure 8 Daily mean melt (± 1 standard error about the mean) of the fen snow-wire versus snow-wire 2 for (a) 1994 and (b) 1995.

Closed-canopy sites (e.g. snow-wire 4) had more protracted melt rates than more open canopies (e.g. snow-wire 5) (Figure 7), as has been observed in other boreal forest studies (e.g. FitzGibbon and Dunne, 1983). Melt at snow-wire 3 (GF = 0.459) was similar to that at snow-wire 5 (GF = 0.659) in 1994, despite the greater exposure at the latter site. This may be due to an understory of labrador tea that was more dense at this site. Price and Dunne (1976) observed that the emergence of branches through a thinning snow cover enhanced melt by increasing both surface roughness (and therefore turbulent fluxes) and absorption of solar radiation, which in turn enhanced the energy available for melt by conduction and longwave radiation. Labrador tea began to protrude through the surface at snow-wire 3 on DOY 110-111 of both years. However, in 1994 this occurred initially on a path running parallel to the snow wire, which in turn may have increased melt rates. The path was rerouted in 1995 to minimize such effects and cumulative melt patterns at snow wires 3 and 5 were consistent with differences in their GF values.

Consistent differences in snowmelt patterns between sites for both years (Figure 7) suggest that a simple discretization between open and forested areas would obscure significant spatial variability in melt. This spatial variability can largely be attributed to differences in canopy density as indicated by gap fraction values at each snow-wire site.

The relationship between snow-wire snowmelt estimates and gap fractions

Table 2 summarizes energy balance data obtained at the fen tower from the initiation of snowmelt to the point when discontinuous snow cover (albedo = 0.37) precluded daily snowmelt estimates. The summary is limited to the 9 day period between DOY 102 and 111 in 1994 and between DOY 101 and 110 in 1995. Total energy available for melt at the fen was 40.4 MJ in 1994 and 22.7 MJ in 1995. Q^* made the dominant contribution to Q_M for both years; however, Q_H fluxes were also significant in 1994 relative to 1995 where a lower Q_H contribution was almost completely offset by Q_E fluxes.

Table 2 Component contributions (MJ) to the total energy flux recorded at the fen tower from the initiation of melt to albedo = 0.37.

	Q^*	Q_H	Q_E	Q_P
1994	30.8	25.9	-16.9	0.6
1995	22.2	11.2	-10.7	0.0

Relationships between average snowmelt rates at each snow-wire in 1994 and 1995 and their respective gap fractions are illustrated in Figure 9. They indicate that differences in climatic conditions and energy available for melt between years do not translate to equally proportional changes in melt rates under different canopy densities. As total Q_M decreased from 1994 to 1995, average melt rate decreased with decreasing canopy density (fen and site 2 snow-wires), but changed little in areas of dense canopy cover (snow wire 4). Figure 9 suggests that the form of the best-fit relationship between melt and gap fraction can vary depending on meteorological conditions during snowmelt.

Best-fit regression relationships (linear, exponential or quadratic) were established between GF (independent variable) and daily snowmelt (dependent variable), and the following options were used to estimate daily melt for the basin:

(i) If the regression coefficient was statistically-significant (α = 0.05), daily snowmelt was estimated by the regression model using a site's GF value;

(ii) If only the intercept coefficient was statistically-significant (α = 0.05), the mean daily snowmelt was calculated and distributed evenly over the basin;

(iii) If neither coefficient was statistically-significant, no melting was assumed for that day.

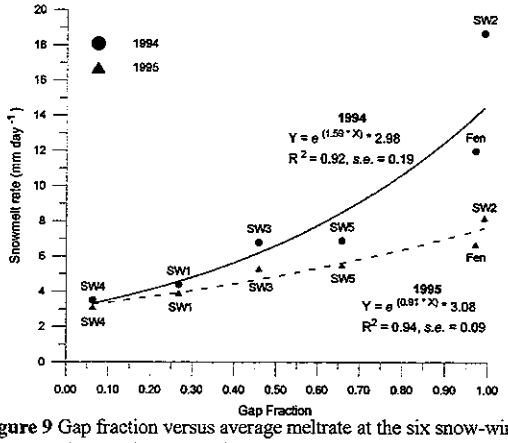

Figure 9 Gap fraction versus average meltrate at the six snow-wire sites, showing the line of best fit for each year (significant at the α = 0.05 level).

Deriving spatially-distributed gap fractions, SWE, and snowmelt rates

i) Gap fractions

Landsat Thematic Mapper (TM) imagery obtained on February 10, 1994 was used to derive a canopy closure index (CCI) using an unsupervised spectral unmixing model (e.g. Rosenthal and Dozier, 1996). The model is based on the high spectral contrast provided by the underlying snowpack that, consequently, makes it highly sensitive to canopy density (Davis *et al.*, 1997). The CCI image was georeferenced with the basin coordinate system using 13 control points obtained from the DVP in a transformation with a RMS error of 12.9 m. Values corresponding to the snow-wire locations were extracted from the CCI image and the best-fit regression relation between CCI and GF values was (Figure 10):

$$GF(\%) = 41.4 \bullet \ln(100 - CCI(\%)) - 84.1;\ R^2 = 0.99;\ s.e. = 4.2 \qquad (4)$$

Snow-wire 3 was considered anomalous and not used in the regression analysis since its location between a forested and open area could result in the surface reflectance being weighted towards the forested area, thus overestimating canopy closure. Also, the LAI-2000 may have 'seen' a gap in one direction while simultaneously 'seeing' dense canopy in the other direction, which could result in overestimation of the gap fraction (Strachan and McCaughey, 1996); however, such errors were minimized by use of the 90° lens cap. The log-linear relationship, similar to those found between leaf area index (LAI) and TM reflectance values (e.g. Running *et al.*, 1989; Spanner *et al.*, 1990), is characteristic of comparisons between 3-dimensional architectural data and results derived from 2-dimensional surface reflectance values. The CCI image was transformed using equation 4 to produce a gap fraction image, the upper and lower bounds of which were constrained to the minimum and maximum gap fractions measured at the snow-wires (0.063 and 0.992, respectively). The resulting gap fraction image (Figure 11) compares well with the basin air photo (Figure 1).

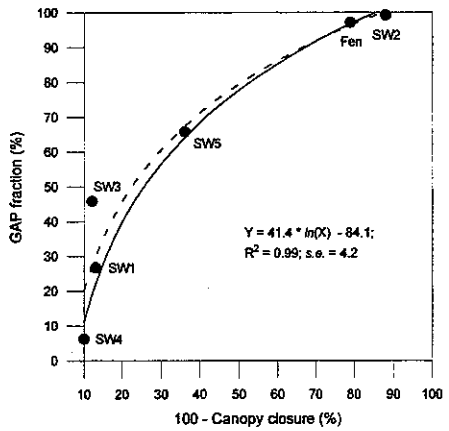

Figure 10 The relationship between gap fraction measurements at the snow-wires and the canopy closure index derived from Landsat TM data. The dashed line is the relationship based on all points while the solid line is the relationship excluding snow-wire 3.

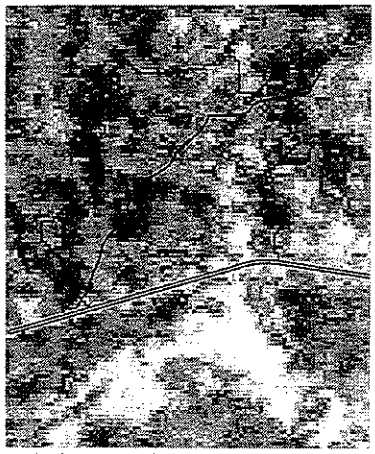

Figure 11 Distributed gap fractions (expressed as %s) ranging between 99% (lightest) and 6% (darkest). The basin divide, the fen to the south of the catchment, Highway 391, and the cutline are shown for reference (see Figure 1).

ii) SWE

Processes governing snow accumulation such as snowfall redistribution by wind, interception and the subsequent sublimation are complex and cannot be easily related to canopy characteristics. A forest canopy opening might have the same gap fraction as an open wetland but the sites would represent the two different extremes of SWE values. Airflow perturbations caused by a canopy opening would promote snow accumulation whereas part of the snowfall received in a wind-swept wetland would be redistributed to the wetland fringes. The magnitude of

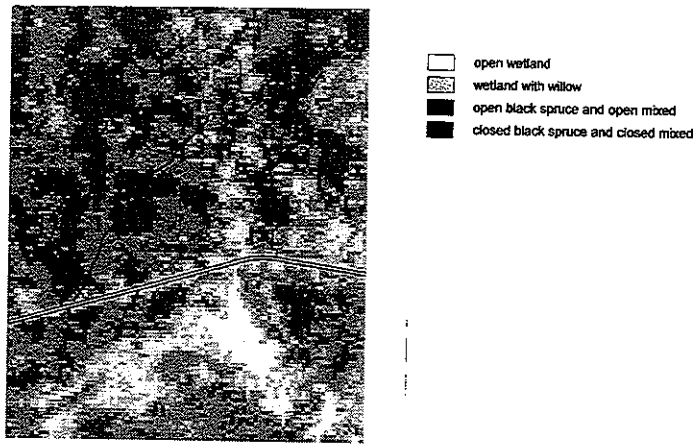

Figure 12 Classification of the gap fraction image (Figure 11) into vegetation units used for distribution of SWE.Classification of the gap fraction image (Figure 11) into vegetation units used for distribution of SWE.

Table 3 Error Matrix Analysis of the minimum distance (normalized) classification of the gap fraction image.

	Wetland	Wetland with willow	Black spruce and mixed	Open black spruce and open mixed	Errors of commission
Wetland	16	7	0	0	0.3043
Wetland with willow	4	11	1	0	0.3125
Black spruce and mixed	0	0	17	3	0.1500
Open black spruce and open mixed	0	2	2	17	0.1905
Errors of omission	0.2000	0.4500	0.1500	0.1500	0.2375

redistribution of snow by wind in a forest opening would be a function of tree height and the size of the opening. The absence of a statistically-significant relationship between the snow survey SWE values (using coordinates obtained from the DVP) and the associated gap fractions illustrate this point.

However, a significant difference between gap fractions of vegetation units discretized in Table 1 permits classification of the gap fraction image into the same vegetation units. This provides a semi-distributed SWE that improves on the use of a mean basin value. Coordinates of twenty training sites were obtained from the DVP for each vegetation unit and signature files produced. Because only one image was used to create signature files and for the subsequent classification, a minimum distance to means classifier was used. This was normalized using standard deviations to account for variability in the signatures. The proportion of the basin consisting of the different vegetation units given in Table 1 was obtained from this classification, which is shown in Figure 12 with an error analysis in Table 3. Although the wetland with willow SWE was not significantly different from th of the open black spruce and open mixed forest units, its surface reflectance and subsequently derived gap fraction were significantly different, thus warranting separate classification. Errors of omission (where training sites of a particular vegetation unit were misclassified) in Table 3 reveal that the major source of error was in the classification of wetland with willow. As previously noted, the TM Imagery was obtained in February of 1994, when much of the willow in the wetlands had already acted as efficient accumulators of snow, were less exposed, and therefore had reflectance values similar to those from the open wetland areas. This resulted in an underestimation of the CCI. Thirty-five percent of wetland with willow sites were misclassified as open wetland, resulting in underestimation of total basin SWE and overestimation of the snowmelt rates in these areas.

iii) Snowmelt rates

Distributed daily snowmelt for each pixel of the GF image was determined using option (i), (ii) or (iii) described above. Melt values were used to calculate the remaining SWE for each pixel on a daily time step beginning with the pre-melt SWE image. SWE values were carried forward on days with no melt. Selected images for 1994 and 1995 are shown in Figure 13. Cumulative melt (Figures 14a and 14b) and snow-covered area (Figure 14c) is compared between vegetation units, and ablation patterns for each vegetation unit with respect to the basin cumulative melt are shown in Figure 14d.

Open wetlands were the first to become snow-free in both years and were fully ablated before the first areas of wetland with willow became snow-free one day later. Similarly, areas of open black spruce and open mixed forest first became snow-free on the same day that the wetland with willow was fully ablated followed by the initial exposure of the closed forest areas 3 days later in 1994 and 1 day later in 1995. Changes in SWE and snow-covered area are shown as the open wetlands (Figures 13a and 13d), wetland with willow (Figures 13b and 13e), and open forested units (Figures 13c and 13f) became snow-free. Although the closed forest areas represented the largest snow-covered area by the end of melt, in both years they became snow-free one day before the last remaining pockets of open forested areas. The latter contained a higher initial SWE and a lower gap fraction in comparison to the mean for the vegetative unit as classified for the SWE distribution. The higher SWE in the open forest areas results in a proportional cumulative melt similar to the closed forest areas despite the higher melt rates (Figures 14a and 14b). Therefore, most of the catchment area receives inputs of meltwater for the duration of the springmelt. The more protracted snowmelt in 1995 is evident (Figures 14a and 14b), and the relatively greater importance of Q_H to Q_M in the initial days of melt in 1994 is suggested by the rapid loss of snow cover in the open wetlands compared to the basin cumulative melt (Figure 14d).

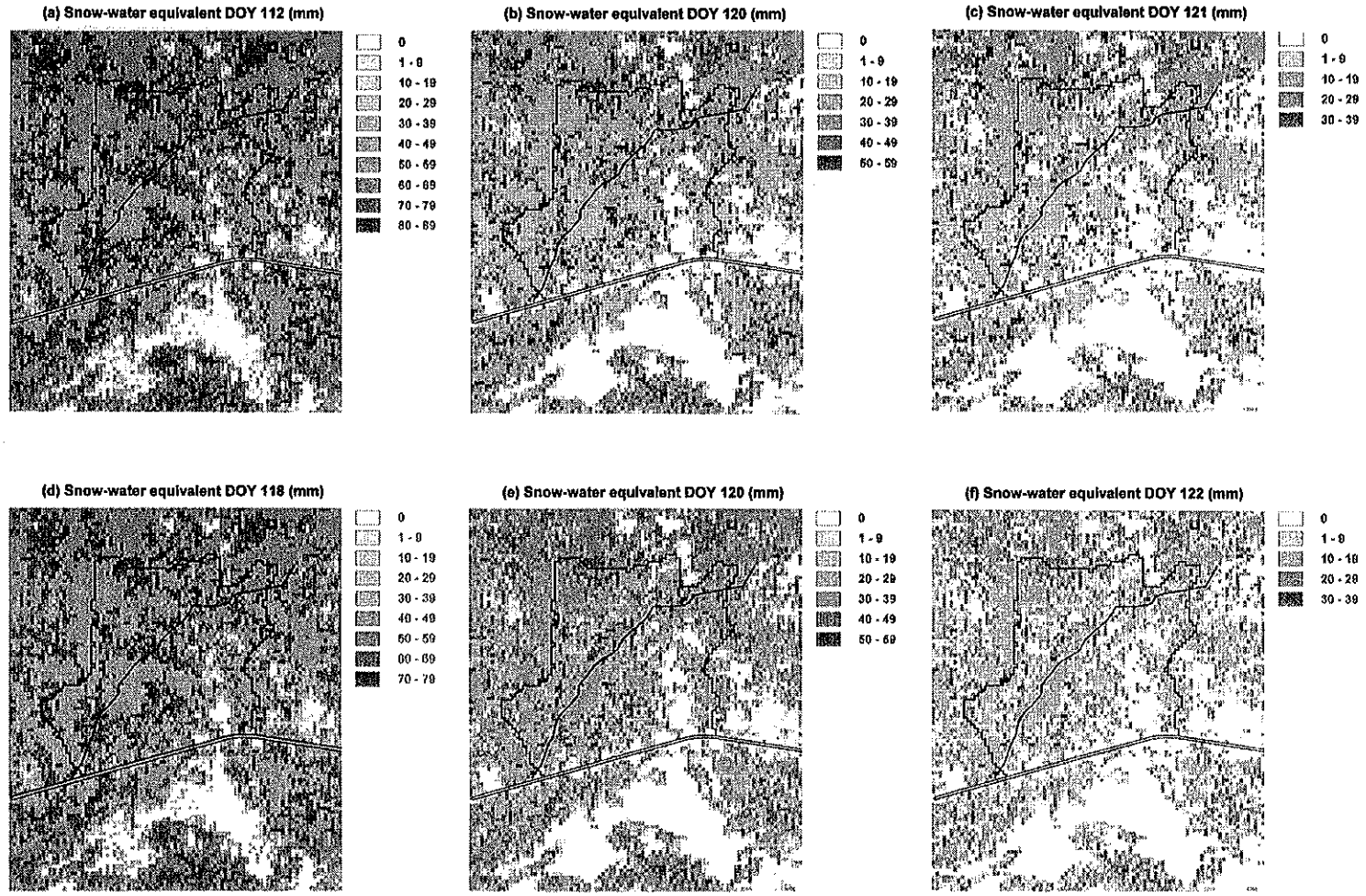

Figure 13 Spatially-distributed estimates of SWE on DOY (a) 112, (b) 120, (c) 121 of 1994 and DOY (d) 118, (e) 120, and (f) 122 of 1995.

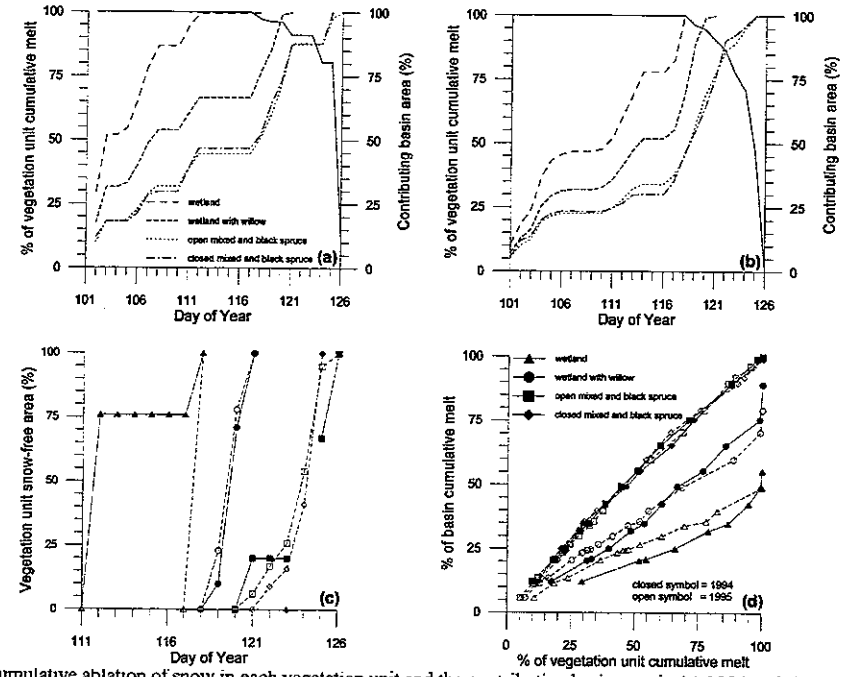

Figure 14 Cumulative ablation of snow in each vegetation unit and the contributing basin area in (a) 1994 and (b) 1995 as well as (c) snow-covered area and (d) ablation patterns with respect to total basin cumulative melt.

CONCLUSIONS

Spatial variation in snowmelt rates in the boreal forest can be explained by differences in canopy density and their effects on: (1) the penetration of solar radiation to the snowpack surface; (2) wind speed, and therefore the turbulent fluxes; and (3) nocturnal radiation losses. This results in a relationship between gap fractions (an indirect measure of canopy density) and daily snowmelt that can follow a linear, exponential or quadratic model. Reduction of snowmelt energy balance components caused by greater canopy density outweighs any increases in longwave radiation as has been observed at other boreal forest sites (e.g. Davis *et al.* , 1997); however, this disagrees with assumptions in other snowmelt models (e.g. Yamazaki and Kondo, 1992). Canopy density derived from Landsat Thematic Mapper imagery can be used as the spatial fabric for the physically-based distribution of daily snowmelt. This distribution produced comparable patterns of snow cover ablation between years with very different climatological conditions. Thus, this work presents a physically-meaningful approach for the scaling-up of point hydrologic processes and properties required as part of BOREAS, and provides the opportunity to test and validate snowmelt models that incorporate canopy density parameters. It also facilitates comparison of the spatio-temporal delivery of snowmelt water to the soil interface and basin discharge in an effort to improve our understanding of runoff processes in the boreal forest.

ACKNOWLEDGEMENTS

This research was funded through grants from the Natural Sciences and Engineering Research Council of Canada, Queen's University and the Northern Scientific Training Program. We are grateful to Dr. R. Davis of the U.S. Army Cold Regions Research and Engineering Laboratory for supplying the CCI image. We wish to thank Greg Bryant, Paul Bartlett, Åsa Chong as well as other BOREAS researchers and support staff for assistance in the field. Logistical support provided through BOREAS is also gratefully acknowledged.

REFERENCES

Adams, W.P. 1976. 'Areal differentiation of snowcover in east central Ontario', *Water Resources Research*, **12**, 1226-1234.

Burkard, M.B., H.R. Whiteley, H.O. Schroeter, and Donald, J.R. 1991. Snow depth/area relationships for various landscape units in southwestern Ontario. *Proceedings of the Eastern Snow Conference*, **48**, 51-65.

Buttle, J.M. and McDonnell, J.J. 1987. Modelling the areal depletion of snowcover in a forested catchment, *Journal of Hydrology*, **90**, 43-60.

Davis, R.E., Hardy, J.P., Ni, W., Woodcock, C., McKenzie, J.C., Jordan, R., and Li, X. 1997. Variation of snow cover ablation in the boreal forest: A sensitivity study on the effects of conifer canopy, *Journal of Geophysical Research*, in press.

FitzGibbon, J.E. and Dunne, T. 1983. Influence of subarctic vegetation cover on snowmelt, *Physical Geography*, **4**, 61-70.

Hardy, J.P., Davis, R.E., Jordan, R., Li, X., Woodcock, C., Ni, W., and McKenzie, J.C. 1997. Snow ablation modelling at the stand scale in a boreal jack pine forest, *Journal of Geophysical Research*, in press.

Hendrick, R.L., Filgate, B.D., and Adams, W.M. 1971. Application of environmental analysis to watershed snowmelt, *Journal of Applied Meteorology*, **10**, 418-429.

Heron, R., and Woo, M-K. 1978. Snowmelt computations for a high Arctic site, *Proceedings of the Eastern Snow Conference*, **35**, 162-172.

Hydrological Atlas of Canada, 1978. Fisheries and Environment Canada, Ottawa.

Koh, G., and Jordan, G. 1995. Sub-surface melting in a seasonal snow cover, *Journal of Glaciology*, **41(139)**, 474-482.

Metcalfe, R.A., and Buttle, J.M. 1995. Controls of canopy structure on snowmelt rates in the boreal forest. *Proceedings of the Eastern Snow Conference*, **52**, 249-257.

Price, A.G. 1988. Prediction of snowmelt rates in a deciduous forest, *Journal of Hydrology*, **101**, 145-157.

Price, A.G., and Dunne, T. 1976. Energy balance computations of snowmelt in a subarctic area, *Water Resources Research*, **12**, 686-694.

Rosenthal, W., and Dozier, J. 1996. Estimating alpine snow cover with unsupervised spectral unmixing. Proceedings IGARSS'96, 2252-2254.

Running, S.W., Nemani, R.R., Peterson, D.L., Band, L.E., Potts, D.F., Pierce, L.L., and Shanner, M.A. 1989. Mapping regional forest evapotranspiration and photosynthesis by coupling satellite data with ecosystem simulation, *Ecology*, **70(4)**, 1090-1101.

Sellers, P., Hall, F., Margolis, H., Kelly, B., Baldocchi, D., den Hartog, G., Cihlar, J., Ryan, M., Goodison, B., Crill, P., Jon Ranson, K., Lettenmaier, D., and Wickland, D. 1995. The Boreal Ecosystem-Atmosphere Study (BOREAS): An Overview and Early Results from the 1994 Field Year, *Bulletin of the American Meteorological Society*, **76(9)**, 1549-1577.

Spanner, M.A., Pierce, L.L, Peterson, D.L., and Running, S.W. 1990. Remote sensing of temperate coniferous forest leaf area index: The influence of canopy closure, understorey vegetation and background reflectance, *International Journal of Remote Sensing*, **11(1)**, 95-111.

Schmidt, R.A. 1991. Sublimation of snow intercepted by an artificial conifer, *Agricultural and Forest Meteorology*,**54**, 1-27.

Strachan, I.B., and McCaughey, J.H. 1996. Spatial and vertical leaf area index of a deciduous forest resolved using the LAI-2000 plant canopy analyzer, *Forest Science*, **42(2)**, 176-181.

Welles, J.M., and Norman, J.M. 1991. An instrument for indirect measurement of canopy architecture, *Agronomy Journal*, **83**, 818-825.

Woo, M-K and Marsh, P. 1978. Analysis of error in the determination of snow storage for small high Arctic basins, *Journal of Applied Meteorology*, **17**, 1537-1541.

Yamazaki, T., and Kondo, J. 1992. The snowmelt and heat balance in snow-covered forested areas, *Journal of Applied Meteorology*, **31**, 1322-1327.